Improved Identification of MS Disease-Relevant Changes in Gray and White Matter using Susceptibility-Based Ultra-High Field MRI

David A. Rudko[1,2], Igor Solovey[2], Joseph S. Gati[2], Marcelo Kremenchutzky[3], and Ravi S. Menon[2]

[1]*Department of Physics and Astronomy, University of Western Ontario, London, Ontario, Canada,* [2]*Robarts Research Institute, Centre for Functional and Metabolic Mapping, London, Ontario, Canada,* [3]*Department of Clinical Neurological Sciences, University of Western Ontario, London, Ontario, Canada*

Target Audience: Researchers using susceptibility-based MRI for characterizing demyelination and iron accumulation in multiple sclerosis (MS).

Purpose: Although MRI is currently employed in diagnosis of MS, its predictive power for evaluating disease progression and monitoring therapy has been very modest[1]. Standard MRI measures of MS disease burden, including number and volume of lesions in white matter, have generally provided inconsistent correlations with clinical metrics such as Extended Disability Status Scale (EDSS), time since clinically isolated syndrome diagnosis (TSCIS) and time since MS diagnosis (TSMS)[1,2]. In this study, we used magnetic susceptibility-based MRI[3] (combined R_2^* and magnetic susceptibility/QS mapping) at 7 T to identify regions of increased iron deposition and decreased myelination in MS patient brain compared to healthy, matched controls. The candidate susceptibility-based MRI biomarkers were correlated with EDSS, TSCIS, TSMS and age to evaluate their suitability as surrogate measures of disease status.

Methods: Informed consent was obtained from a population of 25 patients with either clinically isolated syndrome (4 patients) or relapsing-remitting MS (21 patients), as well as from 15 healthy, age and gender-matched volunteers. Mean age of patients was 37.3, with ages ranging from 21 to 45. Patients had EDSS scores ranging from 0 to 6.

Imaging was performed on a 7 T MRI scanner using: (i) a 3D multi-echo, gradient echo (GRE) sequence to obtain susceptibility-based images (ii) a T_2-weighted, MP-FLAIR sequence for lesion delineation and (iii) a T_1-weighted, MPRAGE acquisition for anatomical reference. Voxel based-morphometry was then applied in the MNI-1 mm space with a general, additive linear model (GLM) to evaluate statistically significant changes in both R_2^* and QS between group-averaged patient and control maps. Age was included as a covariate in the GLM. To investigate the correspondence between the volume of damaged white matter (WM) highlighted in the Z-score maps (Fig. 1) and MS clinical metrics, the volume of damaged WM satisfying a Z<-2.0 criterion for both QS and R_2^* Z-score maps was correlated with three MS clinical metrics: EDSS, TSCIS and TSMS. We also evaluated changes in *mean value* of R_2^* and QS in four sub-cortical gray matter structures (caudate nucleus, putamen, globus pallidus and thalamus). Specifically, the strength of univariate correlations between R_2^* and QS and the three MS clinical metrics was quantified with the effect of age removed.

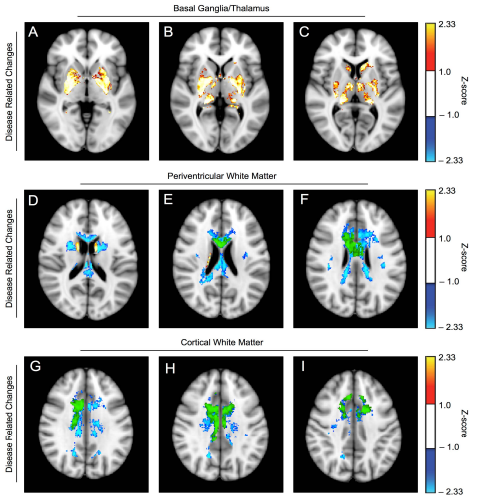

Figure 1: QS-based, axial Z-score maps derived from GLM analysis. Blue colours indicate significantly reduced QS (Z<-1.0) in lesioned tissue of patients compared to controls. Green colours indicate regions of patient normal-appearing white matter (NAWM) with significantly reduced QS (Z<-1.0) compared to controls. Red/orange areas with positive Z-scores indicate brain regions where patients have higher QS (Z > 1.0) compared to controls.

MRI-Derived Parameter	EDSS	TSCIS	TSMS	Age
Caudate R_2^* (1/s)	0.57 (< 0.01)	0.40 (< 0.01)	0.19 (0.18)	0.37 (0.05)
Putamen R_2^* (1/s)	0.39 (< 0.01)	0.21 (0.14)	0.03 (0.86)	0.48 (0.01)
Globus Pallidus R_2^* (1/s)	0.50 (< 0.01)	0.47 (< 0.001)	0.39 (< 0.01)	0.52 (< 0.01)
Thalamus R_2^* (1/s)	0.57 (< 0.01)	0.20 (0.15)	0.06 (0.69)	0.25 (0.21)
Caudate QS (ppb)	0.44 (< 0.01)	0.17 (0.24)	0.06 (0.70)	0.19 (0.32)
Putamen QS (ppb)	0.58 (< 0.001)	0.38 (< 0.01)	0.35 (0.01)	0.39 (0.03)
Globus Pallidus QS (ppb)	0.70 (< 0.001)	0.42 (< 0.01)	0.21 (0.14)	0.59 (< 0.001)
Thalamus QS (ppb)	0.56 (< 0.001)	0.47 (< 0.001)	0.30 (0.04)	0.28 (0.23)

Table 1: Pearson linear correlation between *mean* MRI-derived susceptibility parameters in sub-cortical gray matter and MS clinical metrics. All MRI susceptibility parameters were corrected for age-related increases in iron. Data in parentheses are P values.

Results and Discussion: QS maps identified statistically significant, voxel-level increases in iron deposition in sub-cortical gray matter of MS patients compared to controls (Fig. 1A-C). These voxel-level increases were not observed on R_2^* maps. Region of interest analysis of mean R_2^* and QS in sub-cortical gray matter (Table 1) demonstrated R_2^* ($R \geq 0.39$, $p<0.01$) and QS ($R \geq 0.44$, $p<0.01$-0.001) were strongly correlated with EDSS and also independently predicted TSCIS in some of the sub-cortical nuclei. The volume of total white matter damage (defined by a Z<-2.0 criterion, suggestive of demyelination) on the QS maps of Fig. 1 also correlated significantly with EDSS ($R=0.46$, $p=0.02$). Notably, for the case of QS mapping, the total volume of normal-appearing white matter (NAWM, Z<-2.0 without lesions) damage was significantly larger than that for R_2^*: the per patient NAWM damaged volume calculated from QS was 2126 mm^3 but only 175 mm^3 from R_2^*. This suggests QS may be more sensitive to pre-lesional demyelination in MS patients.

Conclusion: QS and R_2^* maps acquired using standard GRE MRI at high field revealed demyelination and iron accumulation in MS that correlates strongly with clinical disability. Using this information may allow earlier administration of therapies and monitoring of MS pathology in-vivo. Voxel-based QS, was preferentially sensitive to monitoring NAWM demyelination and sub-cortical iron accumulation in-vivo compared to R_2^*. The volume of damaged white matter tissue identified by QS was predictive of EDSS.

References: 1) Moral et al. Archives of Neurology 2009; 66:1345 – 1352. (2) Paty et al. Ann. Neurol. 1994; 36: S95 – 96. (3) Deistung et al. Neuroimage 2013, 65: 299-314.